ACSNANO

www.acsnano.org

ARTICLE

Electrically Tunable Quenching of DNA Fluctuations in Biased Solid-State Nanopores

Hu Qiu,[†,⊥] Anuj Girdhar,[†,‡,⊥] Klaus Schulten,[*,†,‡] and Jean-Pierre Leburton[*,†,‡,§]

[†]Beckman Institute for Advanced Science and Technology, [‡]Department of Physics, and [§]Department of Electrical and Computer Engineering, University of Illinois, Urbana, Illinois 61801, United States

Supporting Information

ABSTRACT: **Nanopores offer sensors for a broad range of nanoscale materials, in particular ones of biological origin such as single- and double-stranded DNA or DNA−protein complexes. In order to increase single-molecule sensitivity, it is desirable to control biomolecule motion inside nanopores. In the present study, we investigate how in the case of a double-stranded DNA the single-molecule sensitivity can be improved through bias voltages. For this purpose we carry out molecular dynamics simulations of the DNA inside nanopores in an electrically biased metallic membrane. Stabilization of DNA, namely, a reduction in thermal fluctuations, is observed under positive bias voltages, while negative voltages bring about only negligible stabilization. For positive biases the stabilization arises from electrostatic attraction between the negatively charged DNA backbone and the positively charged pore surface. Simulations on a teardrop-shaped pore show a transverse shift of DNA position toward the sharp end of the pore under positive bias voltages, suggesting the possibility to control DNA alignment inside nanopores through geometry shaping. The present findings open a feasible and efficient route to reduce thermal noise and, in turn, enhance the signal-to-noise ratio in single-molecule nanopore sensing.**

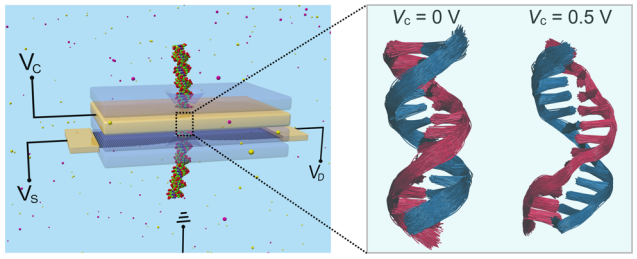

KEYWORDS: *solid-state nanopore, DNA sequencing, molecular dynamics, biosensor, stabilization*

In the past two decades, fast and inexpensive genome sequencing has become a rapidly growing research area.[1−5] DNA sequencing using solid-state nanopores (SSNs), inspired by their biological counterparts,[6−10] holds great promise for genomic applications as a potentially cost-effective, rapid, and scalable technology.[11−15] SSN devices are made of a thin membrane containing one or multiple nanometer-sized pores, through which DNA molecules are translocated under an electric field across the membrane.[16−25] The passing nucleotides in the DNA molecule interact with the membrane, enabling the detection and potentially the identification of individual nucleotides. Typical detection methods include measuring ionic current blockades from DNA dwelling in the nanopore,[7] measuring electrostatic potential changes across a membrane capacitor caused by the passage of DNA charges,[13] and monitoring transverse tunneling currents flowing through nucleotides sandwiched between two membrane electrodes.[26]

Despite many efforts, no practical DNA sequencing experiments using SSNs have been reported so far; detecting a real-time discernible signal for the nucleotides in a DNA strand as the molecule is translocated through SSNs remains a challenging task. One of the primary impediments is the low signal-to-noise ratio due to thermal fluctuations of DNA bases, ions, and water inside SSNs. In particular, the noise from variations in DNA structural conformation inside a nanopore may offset the signal induced by each nucleotide, largely weakening the sensing sensitivity of the nanopore device. Therefore, in order to ensure the effective operation of a nanopore device in single-molecule sensing applications, a scenario to control the motions of biomolecules in SSNs is highly desirable. In biological protein nanopores, the control of motion and translocation velocity of DNA can be achieved by using a processive enzyme, thereby enabling their applications in DNA sequencing,[27] mapping of DNA methylation,[28] and measurement of DNA position within the nanopore with subangstrom precision.[29]

In SSNs, a possible strategy to control molecule motions is the use of a multilayered membrane transistor containing a motion-control electrode layer,[30] as shown in Figure 1a, which shapes the electrostatic landscape in the nanopore to reduce the stochastic fluctuations of the interior biomolecules. To explore this possibility, we carried out computational studies that first self-consistently solve for the electrostatic potential arising from the biased motion-control layer containing two types of nanopores, one with a cylindrical cross section and a second one with a teardrop-shaped cross section. We then performed a

Received: January 11, 2016
Accepted: March 21, 2016
Published: March 21, 2016

DOI: 10.1021/acsnano.6b00226
ACS Nano 2016, 10, 4482−4488

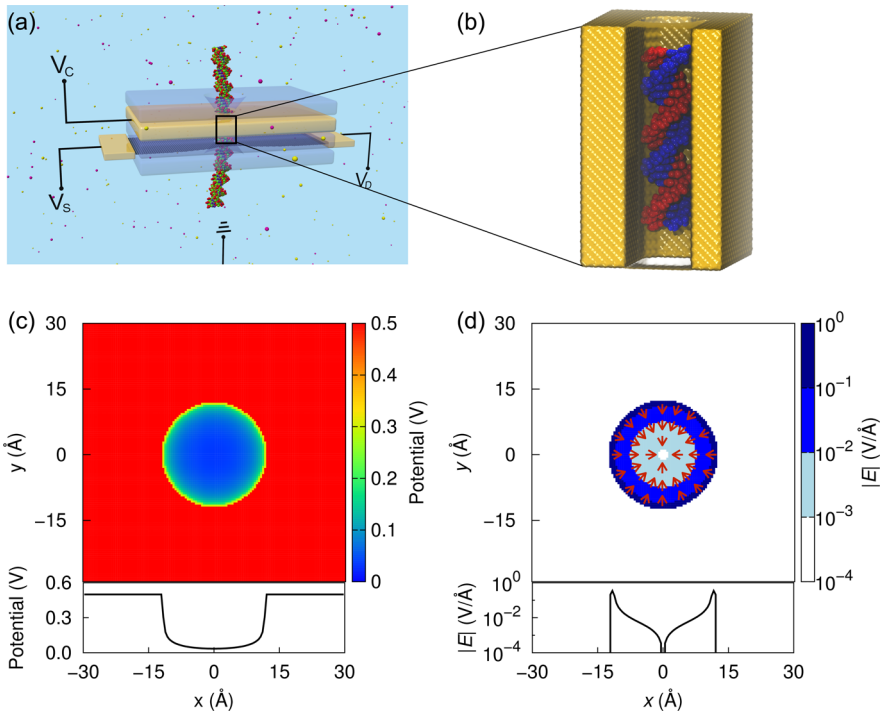

Figure 1. (a) Schematic of a prototypical multilayer transistor with a nanopore for DNA manipulation and detection. A metallic control layer (yellow), sandwiched between two insulating oxide layers (blue), is biased at a voltage V_C. A conducting sensing membrane such as a graphene monolayer, biased at V_D and V_S, is used to detect the passing DNA molecule. The system is biased with respect to a common ground. (b) System of molecular dynamics simulations in this study. The system consists of a dsDNA confined within a nanopore in a metallic membrane. The schematic nanopore shown has a circular cross section. To render the DNA molecule visible, the front part of the membrane is left transparent. (c, d) Electrostatic potential (c) and magnitude of electric field (d) in the *x,y*-plane (top panel) and along a line across the nanopore diameter (bottom panel), of a 0.5 V biased cylindrical nanopore. Arrows denote the directions of local electric fields.

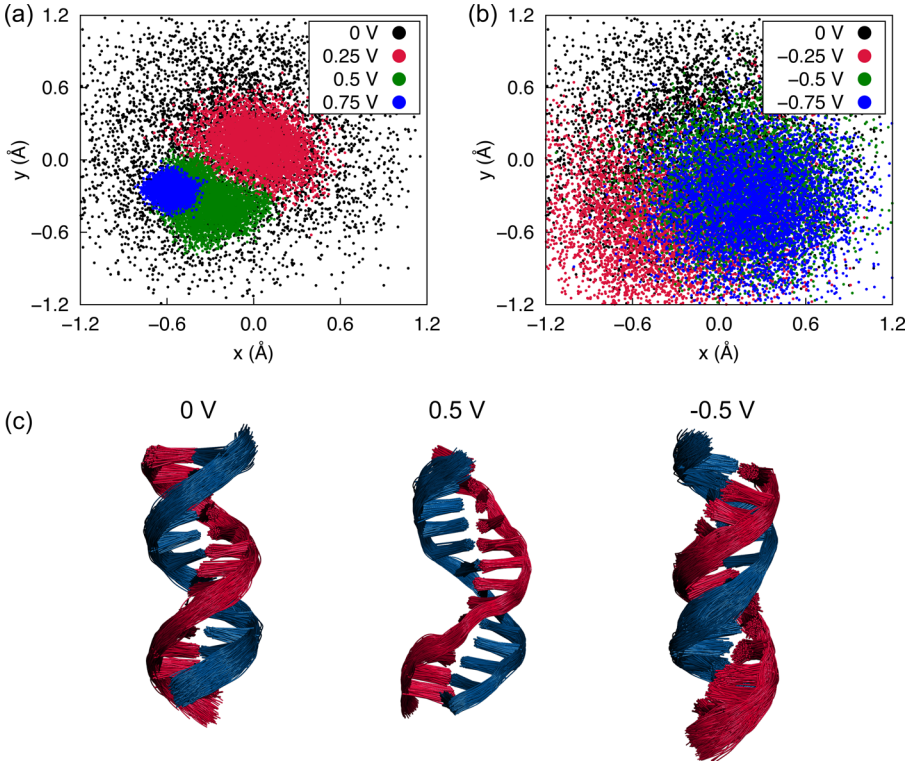

Figure 2. Scatter diagram showing center of mass positions of dsDNA in the last 50 ns of the 70 ns simulation trajectory at (a) positive and (b) negative voltages. (c) Overlapped conformations of the DNA in a 5 ns MD trajectory at 10 ps intervals under voltage biases of 0 (left), 0.5 (middle), −0.5 V (right).

DOI: 10.1021/acsnano.6b00226
ACS Nano 2016, 10, 4482−4488

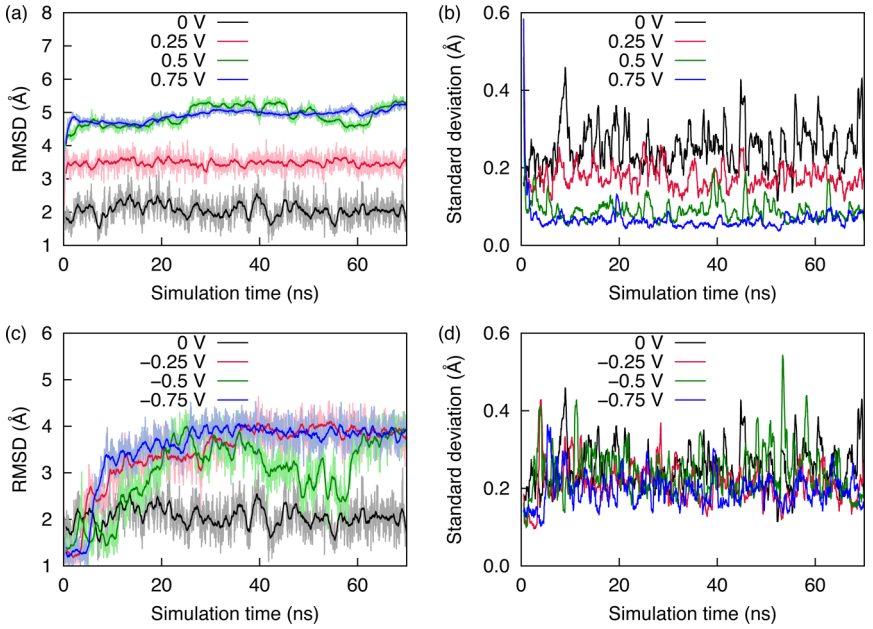

Figure 3. (a, c) RMSDs of all non-hydrogen atoms of the central portion of the dsDNA, namely, nucleotides between the sixth and 17th base-pair of the 22 base-pairs, from the starting DNA conformation in MD simulations at positive (a) and negative (c) bias voltages. The thick lines represent moving average over 100 data points. (b, d) Moving standard deviation over 100 data points of the RMSD for positive (b) and negative (d) voltages.

series of molecular dynamics simulations to determine the effect of the generated electrostatic potential on the motion of a double-stranded DNA (dsDNA) in the nanopore. The results show that DNA fluctuations can be reduced by positive voltage biases higher than 0.5 V, suggesting a promising strategy to stabilize DNA inside nanopores. The reduction of DNA fluctuations could lower the conformational noise in the nucleotide signal measured by a secondary sensing membrane layer and, in turn, improve the sensitivity of nucleotide detection and identification.

RESULTS AND DISCUSSION

We first consider, as shown in Figure 1a, a nanopore in a stacked membrane with a circular cross section and 2.4 nm diameter. In a typical device, the metallic motion-control electrode layer of the stacked membrane is biased at a voltage, V_C, and isolated from the sensing membrane (*e.g.*, graphene) by an oxide layer such as SiO_2[21] or Al_2O_3.[31] In the latter case, a multilayered graphene−Al_2O_3 membrane was fabricated through alternately depositing the layers of graphene and Al_2O_3 onto a substrate.[31] The control voltage is varied from −0.75 V to 0.75 V by applying Dirichlet boundary conditions to the electrode layer, as described in Methods. The control voltage, as well as source (V_S) and drain (V_D) voltages across the sensing membrane, are set with respect to a common ground.[30]

Figure 1c and d show the electrostatic potential and the associated electric field, respectively, in a plane perpendicular to the nanopore axis and at an electrode voltage of 0.5 V. The potential is constant within the metallic interior, but drops rapidly after crossing the pore boundary, due to the large screening of Cl^- ions that are attracted by the positively charged pore surface. The potential along a line through the nanopore center is shown in the bottom panel of Figure 1c. The potential is nearly zero in most regions inside the pore, while a sudden jump near the pore surface is observed, leading to a strong local electric field on the order of 0.1 V/Å (Figure 1d). In addition, the local electric field at every point inside the pore points uniformly to the pore center (Figure 1d). At negative electrode biases, the fields and potentials are identical in magnitude but opposite in sign to those for positive voltages.

The calculated potential was then incorporated in MD simulations to determine its influence on the motion of a dsDNA molecule confined in the pore (Figure 1b). In Figure 2a and b, we show center of mass (CM) positions of the DNA molecule in the *x,y*-plane for each frame in the last 50 ns of 70 ns simulation trajectories at positive and negative voltages, respectively. At zero electrode bias, the DNA positions at different times spread almost uniformly inside the pore, as no significant interaction between the pore and the DNA molecule exists. One also notes that the center point, around which the DNA resides, deviates slightly from the pore center by 0.2 Å, which accounts for about 0.8% of the pore diameter (2.4 nm), due to limited sampling of possible DNA conformations in the MD simulations. At positive voltages (Figure 2a), on the other hand, the DNA CM positions become more localized around a specific location in the pore, indicating damping of the DNA motion around a stable conformation. This location is also not exactly at the pore center because of the slight randomness in conformational change in response to applied voltages. The reduction of DNA fluctuations is discernible through the backbone spread in the overlapped DNA conformations obtained from the MD trajectory at 0.5 V (middle panel in Figure 2c), which is thinner than that in the voltage-free case (left panel). Such a stabilization effect produced by positive voltages is the consequence of electrostatic attraction between the positively charged pore surface and the negatively charged DNA backbone. In addition, larger positive electrode voltages reduce the area within which the DNA CM is found (Figure 2a), suggesting that larger voltages reduce the motion of the DNA molecule more strongly.

DOI: 10.1021/acsnano.6b00226
ACS Nano 2016, 10, 4482−4488

At negative voltages, however, the DNA still fluctuates greatly, as indicated by the broad distribution of DNA CM positions (Figure 2b) and the thicker backbone spread in the DNA conformations (right panel in Figure 2c). The DNA is compressed significantly in the lateral direction due to strong repulsion between the negatively charged pore surface and the DNA backbone. Because DNA is a soft biological molecule, it does not necessarily achieve a perfect symmetric configuration around the pore center after the compression (see the right panel in Figure 2c, for instance). As a result, the scattering of DNA CM positions is centered at a random position, but very close to the pore center. Such randomness in the DNA positions is further supported by another independent series of simulations (see Figure S1 in the Supporting Information), where the DNA CM positions are quite different from those obtained in the above simulations at the same negative voltages. The only difference between the two groups of simulations lies in the seed of a random number generator that was used to assign the initial velocity of each atom in the system.

Figure 3a and c show the root-mean-square deviation (RMSD) profiles of all non-hydrogen atoms of the central portion of the dsDNA from the starting conformation, namely, nucleotides between the sixth and 17th base-pair of the 22 base-pairs, under positive and negative electrode voltages, respectively. In the voltage-free case, the DNA RMSD fluctuates around an average value of 2.1 Å during the whole simulation (black curve in Figure 3a or c), with a high moving standard deviation ranging from 0.2 to 0.5 Å (black curve in Figure 3b or d). When a positive voltage V_C = 0.25 V is applied to the electrode, the overall RMSD profile (red) fluctuates around a relatively larger average displacement of ~3.5 Å from the starting conformation of the DNA (Figure 3a), with a moving standard deviation between 0.15 and 0.3 Å that is reduced compared to the voltage-free case (Figure 3b). The conformational change is attributed to the lateral expansion of the dsDNA in the *x*,*y*-plane of the cylindrical pore that is induced by electrostatic attraction between the positively charged pore surface and the negatively charged DNA backbone. As the positive voltage further increases to V_C = 0.5 V, the DNA RMSD profile exhibits an enhanced conformational change from the starting DNA structure with an average displacement of ~4.7 Å (green). In parallel, the moving standard deviation of the RMSD profile at this voltage is significantly reduced compared to V_C values at 0.25 and 0 V, indicating that the thermal fluctuation of dsDNA is greatly inhibited (see also middle panel in Figure 2c). When the positive voltage is increased to 0.75 V (blue curve in Figure 3a), the dsDNA exhibits comparable RMSD values to those at 0.5 V voltage, indicating that the lateral expansion of the DNA becomes saturated. However, the decreased moving standard deviation observed at 0.75 V electrode voltage suggests that higher positive voltages achieve stronger stabilization (blue curve in Figure 3b). The stabilization at positive voltages is induced by the adhesion of DNA to the pore surface. Once adhered, the DNA molecule cannot detach easily from the pore surface unless a nonpositive voltage is applied, as we document now.

In sharp contrast to the positive electrode biases, no evident stabilization effect is observed when negative voltages are applied to the membrane, as indicated by the large fluctuations in RMSD profiles for all negative voltages (Figure 3c and d). However, the RMSD values are also increased at these negative voltages from the voltage-free case, the increase being induced by the lateral shrinkage of DNA due to electrostatic repulsion between the negatively charged pore surface and DNA backbone (see also right panel in Figure 2c). In all cases for negative voltages, the moving standard deviation displays no significant dependence on voltage strength (Figure 3d), further indicating that negative voltages cannot effectively stabilize the DNA.

A quick response to changes in electrode voltage is of significance in applications where real-time and precise manipulation of biological molecules is required. To assess the possibility, we simulated the response of a DNA molecule to a pulsed voltage of 0.5 V, namely, a voltage turned on and off repeatedly every 30 ns, as depicted in Figure 4a. Figure 4b and c show the moving average and standard deviation of the RMSD of a dsDNA molecule from the initial configuration, respectively. When the voltage is turned on, the lower fluctuations in the RMSD profile (Figure 4b), validated by a lower standard deviation (Figure 4c), indicate the stabilization of DNA in the nanopore. When the voltage is turned off, the DNA reverts, as expected, to a configuration with lower RMSDs, but larger fluctuations. When the positive voltage is turned on again, the fluctuations are again suppressed. In addition, it is worth mentioning that the stabilization is achieved within 1 ns after turning on the voltage, indicating the ability of a real-time and precise manipulation to DNA motion.

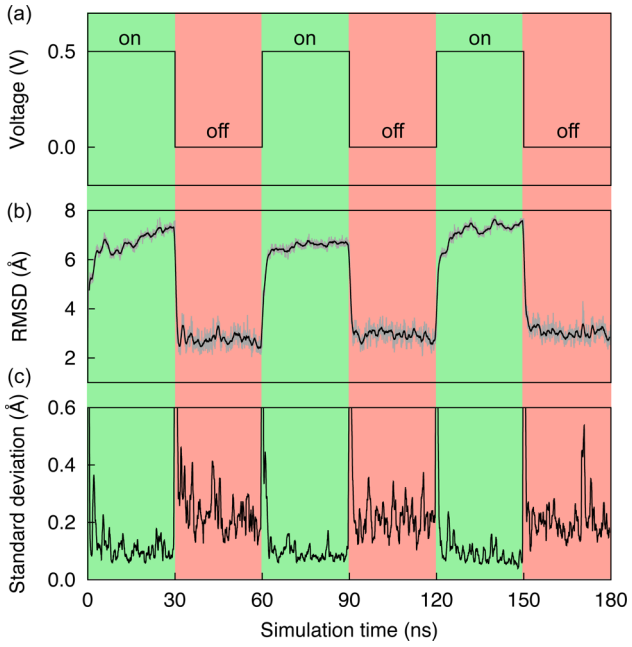

Figure 4. Controllable stabilization of DNA by a pulsed voltage of 0.5 V. (a–c) Voltage applied to the electrode (a), calculated RMSD from the starting configuration (b), and the associated standard deviation (c) *versus* simulation time.

In all the above simulations, a circular pore was considered to confine DNA and generate the potential landscape for DNA stabilization. As expected, the dwelling area of the DNA CM positions inside such a symmetric pore is approximately circular (Figure 2). In realistic experiments, however, a fabricated pore hardly turns out to be a perfect cylinder. For instance, nanopores drilled into solid-state membranes, by focused ion beams,[32] high-energy electron beams,[33] or dielectric breakdown,[34] adopt cross sections that are irregularly shaped and not symmetric around the pore center. In this context, one may

DOI: 10.1021/acsnano.6b00226
ACS Nano 2016, 10, 4482–4488

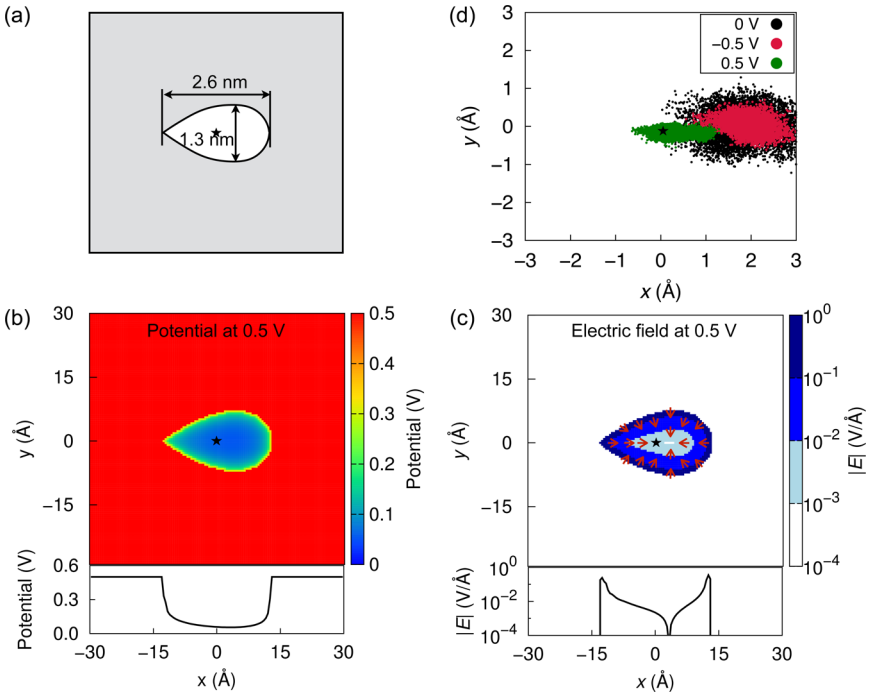

Figure 5. Customized control of DNA alignment through pore geometry shaping. (a) Geometry of the cross section of the teardrop-shaped nanopore simulated in the present study. (b, c) Electrostatic potential (b) and magnitude of electric field (c) of the teardrop-shaped nanopore at 0.5 V electrode voltage, in the *x*,*y*-plane (top panel) and along a line across the center and the sharp end of the pore (bottom panel). The nanopore center is defined as *x*,*y* = 0,0 and depicted as a star. (d) Scatter diagram showing center of mass positions of DNA in MD simulations at electrode voltages of 0, 0.5, and −0.5 V.

wonder if a pore with a lower spatial symmetry can achieve a customized control on the DNA conformation. For this purpose, we consider a teardrop-shaped pore to assess the influence of the pore geometry on DNA behavior, as shown in Figure 5a. In Figure 5b and c, we show the electrostatic potential and electric field for a teardrop-shaped nanopore, respectively, at a positive electrode voltage of 0.5 V. Potential and electric field are no longer symmetric in the *x*-direction, but rather decay more slowly away from the sharp end (left) than from the smooth end (right) of the teardrop circumference. When the obtained potential is applied to the DNA molecule, a strong DNA localization occurs again, as seen from the concentrated distribution of CM positions (green dots in Figure 5d) compared to the voltage-free case (black dots in Figure 5d). In addition, it is worth noting that the DNA moves slightly leftward to approach the sharp end under the positive voltage, mainly due to the relatively higher magnitude and slower decay of the potential/electric field on the left side of the pore. At a negative voltage of $V_C = -0.5$ V, the inhibition of DNA fluctuation and the leftward movement of the DNA center are insignificant compared to the positive voltage case. The demonstrated controllable alignment of DNA inside shaped nanopores is of critical importance in DNA sensing applications where a high-sensitivity DNA sensing emerges only when DNA bases are aligned along a specific direction, for example, perpendicular to the flowing direction of the transverse current.[35]

CONCLUSIONS

In summary, we suggest the use of a biased nanopore to quench DNA conformational fluctuations by combining self-consistent electrostatic potential calculations and molecular dynamics simulations. We found that DNA molecules are stabilized by imposing positive voltages higher than 0.5 V on the nanopore electrodes. The reduction of DNA fluctuations is attributed to the electrostatic attraction between the negatively charged DNA backbone and the positively charged pore surface. No evident conformational response of DNA occurs at negative electrode voltages. The use of a teardrop-shaped pore yields also a teardrop-shaped distribution of DNA positions, which shrinks significantly and shifts slightly toward the sharp end of the pore under positive electrode voltages. The present findings open a simple and efficient route to control motions of biological molecules inside nanopores to improve the signal-to-noise ratio, which is highly desirable for nanopore sensing applications.

METHODS

Our methodological approach outlined here includes calculation of the electrostatic potential arising from various voltage biases at the motion-control electrode layer and subsequent classic MD simulations of DNA fluctuations under the obtained potentials, which were applied to the DNA molecule *via* the grid force module of NAMD2.[36]

Electrostatic Potential Calculations. The electrostatic potential ϕ inside a nanopore filled with electrolytic solution was obtained by solving the Poisson−Boltzmann equation in three dimensions:

$$\nabla\cdot[\epsilon(\mathbf{r})\nabla\phi(\mathbf{r})] = -e[c_{K^+}(\mathbf{r}) - c_{Cl^-}(\mathbf{r})] \quad (1)$$

where $\epsilon(\mathbf{r})$ is the position-dependent dielectric constant, *i.e.*, $\epsilon = 78$ in water and $\epsilon \to \infty$ at the metal electrode. The right-hand-side charge term is associated with the distribution of ions in solution (K^+ and Cl^-), which are described assuming a Boltzmann equilibrium, namely, through[13]

$$c_{K^+}(\mathbf{r}) = c_0 \exp(-e\phi(\mathbf{r})/k_BT), \quad c_{Cl^-}(\mathbf{r}) = c_0 \exp(e\phi(\mathbf{r})/k_BT) \quad (2)$$

where c_{K^+} and c_{Cl^-} are the local ion concentrations of K^+ and Cl^- and c_0 is the molar concentration of the solution, taken to be 0.3 M.

DOI: 10.1021/acsnano.6b00226
ACS Nano 2016, 10, 4482−4488

The system was discretized within a Cartesian box onto a nonuniform, rectilinear grid. Neumann boundary conditions were imposed on the sides of the box,

$$\frac{\partial \phi}{\partial x}|_{x=\pm L_x/2} = \frac{\partial \phi}{\partial y}|_{y=\pm L_y/2} = 0 \quad (3)$$

while the top and bottom of the box were subjected to Dirichlet boundary conditions:

$$\phi(z = \pm L_z/2) = \phi_{\pm} \quad (4)$$

where L_x, L_y, and L_z represent the dimensions of the box in x, y, and z directions, respectively. All electrode points were also subjected to Dirichlet conditions, with the potential ϕ set to the given bias voltage.

Equation 1 can be solved self-consistently using a number of methods. In the present study, we adopted a Newton-Multigrid[37−39] method that discretizes the system onto a 129 × 129 × 129 point uniform grid. Starting from the finest grid, Jacobi relaxation was performed to obtain an initial guess for the solution ϕ. Then, the solution was interpolated and relaxed on subsequently coarser grids to smooth out high-frequency errors. Finally, the error to the solution was relaxed and interpolated on finer grids until the original, fine-grid solution was corrected. Once the solution ϕ was obtained, it was reinserted back into the Poisson−Boltzmann equation, and this process was repeated until the desired convergence was reached. A full description of the exact procedure followed has been provided earlier.[37−39]

Molecular Dynamics Simulations. A dsDNA helix containing 22 base-pairs of dA-dT was constructed by the X3DNA program.[40] For the sake of simplicity, we placed the DNA strand, subjected to mathematical boundaries representing the confinement of DNA in a cylindrical or tear-drop shaped nanopore, in a water box. Inclusion of a real material as the motion-control layer, such as copper or gold, would alter the stabilization behavior demonstrated here; in some cases, the stabilization effect may be promoted due to the strong intrinsic interaction between the pore and DNA molecule.

K^+ and Cl^- ions were randomly added to the water box to make the system charge neutral and achieve an ion concentration of 0.3 M. All simulations were carried out with NAMD 2.9[36] and visualized and analyzed with VMD.[41] A Langevin thermostat was adopted to maintain a constant temperature of 300 K. Periodic boundary conditions were imposed in all directions, and, thereby, an infinitely long nanopore was obtained in the z-direction. DNA was described with the CHARMM27[42] force field, and water was modeled by the TIP3P[43] water model. A time step of 2 fs was used in all simulations. The particle-mesh-Ewald method[44] was employed to treat the long-range electrostatic interactions. Van der Waals energies were calculated using a cutoff of 12 Å. After a 5000-step energy minimization, the system was initially equilibrated for 2 ns as an NPT ensemble, in which the Langevin piston method[45] was used to control the pressure at 1 atm. The calculated potential through eq 1 was then applied to the DNA only in the MD simulations, as the redistribution of ions and water by the potential has already been taken into account in the Poisson−Boltzmann solution of eq 1. At a given voltage, each simulation was run for 70 ns as an NVT ensemble for data analysis.

ASSOCIATED CONTENT

Supporting Information

The Supporting Information is available free of charge on the ACS Publications website at DOI: 10.1021/acsnano.6b00226.

Additional simulation results showing the randomness of DNA position distribution at negative electrode voltages (PDF)

AUTHOR INFORMATION

Corresponding Authors

*E-mail: kschulte@ks.uiuc.edu.

*E-mail: jleburto@illinois.edu.

Author Contributions

⊥H. Qiu and A. Girdhar contributed equally to this work.

Notes

The authors declare no competing financial interest.

ACKNOWLEDGMENTS

This work was supported by grants from Oxford Nanopore Technology, the Seeding Novel Interdisciplinary Research Program of the Beckman Institute, National Institutes of Health grant 9P41GM104601, and National Science Foundation grants PHY0822613 and PHY1430124. The authors gratefully acknowledge also supercomputer time provided through the Extreme Science and Engineering Discovery Environment (XSEDE) grant MCA93S028 and by the University of Illinois at Urbana−Champaign on the TAUB cluster.

REFERENCES

(1) Taber, K. A. J.; Dickinson, B. D.; Wilson, M. The Promise and Challenges of Next-Generation Genome Sequencing for Clinical Care. *JAMA Int. Med.* **2014**, *174*, 275−280.

(2) Schadt, E. E.; Turner, S.; Kasarskis, A. A Window into Third-Generation Sequencing. *Hum. Mol. Genet.* **2010**, *19*, R227−R240.

(3) Branton, D.; Deamer, D. W.; Marziali, A.; Bayley, H.; Benner, S. A.; Butler, T.; Di Ventra, M.; Garaj, S.; Hibbs, A.; Huang, X.; Jovanovich, S. B.; Krstic, P. S.; Lindsay, S.; Ling, X. S.; Mastrangelo, C. H.; Meller, A.; Oliver, J. S.; Pershin, Y. V.; Ramsey, J. M.; Riehn, R.; et al. The Potential and Challenges of Nanopore Sequencing. *Nat. Biotechnol.* **2008**, *26*, 1146−1153.

(4) Venkatesan, B. M.; Bashir, R. Nanopore Sensors for Nucleic Acid Analysis. *Nat. Nanotechnol.* **2011**, *6*, 615−624.

(5) Schloss, J. A. How to Get Genomes at One Ten-Thousandth the Cost. *Nat. Biotechnol.* **2008**, *26*, 1113.

(6) Bezrukov, S. M.; Vodyanoy, I.; Brutyan, R. A.; Kasianowicz, J. J. Dynamics and Free Energy of Polymers Partitioning into a Nanoscale Pore. *Macromolecules* **1996**, *29*, 8517−8522.

(7) Kasianowicz, J. J.; Brandin, E.; Branton, D.; Deamer, D. W. Characterization of Individual Polynucleotide Molecules using a Membrane Channel. *Proc. Natl. Acad. Sci. U. S. A.* **1996**, *93*, 13770−13773.

(8) Akenson, M.; Branton, D.; Kasianowicz, J. J.; Brandin, E.; Deamer, D. W. Microsecond Time-Scale Discrimination among Polycytidylic Acid, Polyadenylic Acid, and Polyuridylic Acid as Homopolymers or as Segments Within Singe RNA Molecules. *Biophys. J.* **1999**, *77*, 3227−3233.

(9) Kumar, S.; Tao, C.; Chien, M.; Hellner, B.; Balijepalli, A.; Robertson, J. W.; Li, Z.; Russo, J. J.; Reiner, J. E.; Kasianowicz, J. J.; Ju, J. PEG-Labeled Nucleotides and Nanopore Detection for Single Molecule DNA Sequencing by Synthesis *Sci. Rep.***2012**, *2*, 10.1038/srep00684.

(10) Reiner, J. E.; Balijepalli, A.; Robertson, J. W.; Campbell, J.; Suehle, J.; Kasianowicz, J. J. Disease Detection and Management *via* Single Nanopore-Based Sensors. *Chem. Rev.* **2012**, *112*, 6431−6451.

(11) Xie, P.; Xiong, Q.; Fang, Y.; Qing, Q.; Lieber, C. M. Local Electrical Potential Detection of DNA by Nanowire-Nanopore Sensors. *Nat. Nanotechnol.* **2012**, *7*, 119−125.

(12) Howorka, S.; Siwy, Z. Nanopore Analytics: Sensing of Single Molecules. *Chem. Soc. Rev.* **2009**, *38*, 2360−2384.

(13) Gracheva, M. E.; Xiong, A.; Aksimentiev, A.; Schulten, K.; Timp, G.; Leburton, J.-P. Simulation of the Electric Response of DNA Translocation through a Semiconductor Nanopore-Capacitor. *Nanotechnology* **2006**, *17*, 622−633.

(14) Li, J.; Gershow, M.; Stein, D.; Brandin, E.; Golovchenko, J. DNA Molecules and Configurations in a Solid-State Nanopore Microscope. *Nat. Mater.* **2003**, *2*, 611−615.

(15) Carlsen, A. T.; Zahid, O. K.; Ruzicka, J.; Taylor, E. W.; Hall, A. R. Interpreting the Conductance Blockades of DNA Translocations through Solid-State Nanopores. *ACS Nano* **2014**, *8*, 4754−4760.

DOI: 10.1021/acsnano.6b00226
ACS Nano 2016, 10, 4482−4488

(16) Sathe, C.; Zou, X.; Leburton, J.-P.; Schulten, K. Computational Investigation of DNA Detection using Graphene Nanopores. *ACS Nano* **2011**, *5*, 8842−8851.
(17) Skinner, G. M.; van den Hout, M.; Broekmans, O.; Dekker, C.; Dekker, N. H. Distinguishing Single- and Double-Stranded Nucleic Acid Molecules using Solid-State Nanopores. *Nano Lett.* **2009**, *9*, 2953−2960.
(18) Dekker, C. Solid-State Nanopores. *Nat. Nanotechnol.* **2007**, *2*, 209−215.
(19) Wanunu, M.; Sutin, J.; McNally, B.; Chow, A.; Meller, A. DNA Translocation Governed by Interactions with Solid-State Nanopores. *Biophys. J.* **2008**, *95*, 4716−4725.
(20) Schneider, G. F.; Kowalczyk, S. W.; Calado, V. E.; Pandraud, G.; Zandbergen, H. W.; Vandersypen, L. M. K.; Dekker, C. DNA Translocation through Graphene Nanopores. *Nano Lett.* **2010**, *10*, 3163−3167.
(21) Merchant, C. A.; Healy, K.; Wanunu, M.; Ray, V.; Peterman, N.; Bartel, J.; Fischbein, M. D.; Venta, K.; Luo, Z.; Johnson, A. T. C.; Drndić, M. DNA Translocation through Graphene Nanopores. *Nano Lett.* **2010**, *10*, 2915−2921.
(22) Garaj, S.; Hubbard, W.; Reina, A.; Kong, J.; Branton, D.; Golovchenko, J. A. Graphene as a Subnanometre Trans-Electrode Membrane. *Nature* **2010**, *467*, 190−193.
(23) Qiu, H.; Guo, W. Detecting ssDNA at Single-Nucleotide Resolution by Sub-2-Nanometer Pore in Monoatomic Graphene: A Molecular Dynamics Study. *Appl. Phys. Lett.* **2012**, *100*, 083106.
(24) Liu, K.; Feng, J.; Kis, A.; Radenovic, A. Atomically Thin Molybdenum Disulfide Nanopores with High Sensitivity for DNA Translocation. *ACS Nano* **2014**, *8*, 2504−2511.
(25) Qiu, H.; Sarathy, A.; Leburton, J.-P.; Schulten, K. Intrinsic Stepwise Translocation of Stretched ssDNA in Graphene Nanopores. *Nano Lett.* **2015**, *15*, 8322−8330.
(26) Zwolak, M.; Ventra, M. D. Electronic Signature of DNA Nucleotides *via* Transverse Transport. *Nano Lett.* **2005**, *5*, 421−424.
(27) Manrao, E. A.; Derrington, I. M.; Laszlo, A. H.; Langford, K. W.; Hopper, M. K.; Gillgren, N.; Pavlenok, M.; Niederweis, M.; Gundlach, J. H. Reading DNA at Single-Nucleotide Resolution with a Mutant MspA Nanopore and Phi29 DNA Polymerase. *Nat. Biotechnol.* **2012**, *30*, 349−353.
(28) Laszlo, A. H.; Derrington, I. M.; Brinkerhoff, H.; Langford, K. W.; Nova, I. C.; Samson, J. M.; Bartlett, J. J.; Pavlenok, M.; Gundlach, J. H. Detection and Mapping of 5-Methylcytosine and 5-Hydroxymethylcytosine with Nanopore MspA. *Proc. Natl. Acad. Sci. U. S. A.* **2013**, *110*, 18904−18909.
(29) Derrington, I. M.; Craig, J. M.; Stava, E.; Laszlo, A. H.; Ross, B. C.; Brinkerhoff, H.; Nova, I. C.; Doering, K.; Tickman, B. I.; Ronaghi, M.; Mandell, J. G.; Gunderson, K. L.; Gundlach, J. H. Subangstrom Single-Molecule Measurements of Motor Proteins using a Nanopore. *Nat. Biotechnol.* **2015**, *33*, 1073−1075.
(30) Girdhar, A.; Sathe, C.; Schulten, K.; Leburton, J.-P. Graphene Quantum Point Contact Transistor for DNA Sensing. *Proc. Natl. Acad. Sci. U. S. A.* **2013**, *110*, 16748−16753.
(31) Venkatesan, B. M.; Estrada, D.; Banerjee, S.; Jin, X.; Dorgan, V. E.; Bae, M.-H.; Aluru, N. R.; Pop, E.; Bashir, R. Stacked Graphene-Al_2O_3 Nanopore Sensors for Sensitive Detection of DNA and DNA-Protein Complexes. *ACS Nano* **2011**, *6*, 441−450.
(32) Gershow, M.; Golovchenko, J. A. Recapturing and Trapping Single Molecules with a Solid-State Nanopore. *Nat. Nanotechnol.* **2007**, *2*, 775−779.
(33) Storm, A. J.; Chen, J. H.; Ling, X. S.; Zandergen, H. W.; Dekker, C. Fabrication of Solid-State Nanopore with Single-Nanometre Precision. *Nat. Mater.* **2003**, *2*, 537−540.
(34) Yanagi, I.; Akahori, R.; Hatano, T.; Takeda, K.-i. Fabricating Nanopores with Diameters of Sub-1 to 3 nm using Multilevel Pulse-Voltage Injection. *Sci. Rep.* **2014**, *4*, 5000.
(35) Girdhar, A.; Sathe, C.; Schulten, K.; Leburton, J.-P. Tunable Graphene Quantum Point Contact Transistor for DNA Detection and Characterization. *Nanotechnology* **2015**, *26*, 134005.
(36) Phillips, J. C.; Braun, R.; Wang, W.; Gumbart, J.; Tajkhorshid, E.; Villa, E.; Chipot, C.; Skeel, R. D.; Kale, L.; Schulten, K. Scalable Molecular Dynamics with NAMD. *J. Comput. Chem.* **2005**, *26*, 1781−1802.
(37) Trottenberg, U.; Oosterlee, C. W.; Schuller, A. *Multigrid*; Academic Press, 2000.
(38) Briggs, W. L.; McCormick, S. F. *A Multigrid Tutorial*; Siam, 2000.
(39) Press, W. H.; Teukolsky, S. A.; Vetterling, W. T.; Flannery, B. P. *Numerical Recipes in C (2nd Ed.): The Art of Scientific Computing*; Cambridge University Press: New York, NY, USA, 1992.
(40) Lu, X.-J.; Olson, W. K. 3DNA: A Software Package for the Analysis, Rebuilding and Visualization of Three-Dimensional Nucleic Acid Structures. *Nucleic Acids Res.* **2003**, *31*, 5108−5121.
(41) Humphrey, W.; Dalke, A.; Schulten, K. VMD - Visual Molecular Dynamics. *J. Mol. Graphics* **1996**, *14*, 33−38.
(42) MacKerell, A. D., Jr.; Bashford, D.; Bellott, M.; Dunbrack, R. L., Jr.; Evanseck, J. D.; Field, M. J.; Fischer, S.; Gao, J.; Guo, H.; Ha, S.; Joseph, D.; Kuchnir, L.; Kuczera, K.; Lau, F. T. K.; Mattos, C.; Michnick, S.; Ngo, T.; Nguyen, D. T.; Prodhom, B.; Reiher, I. W. E.; et al. All-Atom Empirical Potential for Molecular Modeling and Dynamics Studies of Proteins. *J. Phys. Chem. B* **1998**, *102*, 3586−3616.
(43) Jorgensen, W. L.; Chandrasekhar, J.; Madura, J. D.; Impey, R. W.; Klein, M. L. Comparison of Simple Potential Functions for Simulating Liquid Water. *J. Chem. Phys.* **1983**, *79*, 926−935.
(44) Essmann, U.; Perera, L.; Berkowitz, M. L.; Darden, T.; Lee, H.; Pedersen, L. G. A Smooth Particle Mesh Ewald Method. *J. Chem. Phys.* **1995**, *103*, 8577−8593.
(45) Feller, S. E.; Zhang, Y.; Pastor, R. W.; Brooks, B. R. Constant Pressure Molecular Dynamics Simulation: The Langevin Piston Method. *J. Chem. Phys.* **1995**, *103*, 4613−4621.

DOI: 10.1021/acsnano.6b00226
ACS Nano 2016, 10, 4482−4488